Fermi surface reconstruction of superoxygenated La_2CuO_4 superconductors with ordered oxygen interstitials

Thomas Jarlborg[1] and Antonio Bianconi[2,3,4]

[1]*DPMC, University of Geneva, 24 Quai Ernest-Ansermet, CH-1211 Geneva 4, Switzerland*

[2]*RICMASS Rome International Center for Materials Science Superstripes, Via dei Sabelli 119A, 00185 Rome, Italy*

[3]*Institute of Crystallography, Consiglio Nazionale delle Ricerche, via Salaria, 00015 Monterotondo, Italy*

[4]*Physics Department, Sapienza University of Rome, 00185 Rome, Italy*

(Received 6 November 2012; revised manuscript received 18 February 2013; published 28 February 2013)

Novel imaging methods show that the mobile dopants in optimum doped La_2CuO_{4+y} (LCO) get self-organized, instead of randomly distributed, to form an inhomogeneous network of nanoscale metallic puddles with ordered oxygen interstitials interspersed with oxygen-depleted regions. These puddles are expected to be metallic, being far from half filling because of high dopant density, and to sustain superconductivity having a size in the range 5–20 nm. However, the electronic structure of these heavily doped metallic puddles is not known. In fact the rigid-band model fails because of ordering of dopants and supercell calculations are required to obtain the Fermi surface reconstruction. We have performed advanced band calculations for a large supercell $La_{16}Cu_8O_{32+N}$ where $N = 1$ or 2 oxygen interstitials form rows in the spacer $La_{16}O_{16+N}$ layers intercalated between the CuO_2 layers as determined by scanning nano x-ray diffraction. The additional occupied states made by interstitial oxygen orbitals sit well below the Fermi level (E_F) and lead to hole doping as expected. The unexpected results show that in the heavily doped puddles the altered Cu($3d$)-O($2p$) band hybridization at E_F induces a multiband electronic structure with the formation of multiple Fermi surface spots: (a) Small gaps appear in the folded Fermi surface, (b) three minibands cross E_F with reduced Fermi energies of 60, 150, and 240 meV, respectively, (c) the density of states and band mass at E_F show substantial increases, and (d) spin-polarized calculations show a moderate increase of antiferromagnetic spin fluctuations. All calculated features are favorable to enhance superconductivity; however, the comparison with experimental methods probing the average electronic structure of cuprates will require the description of the electronics of a network of multigap superconducting puddles.

DOI: 10.1103/PhysRevB.87.054514 PACS number(s): 74.20.Pq, 74.25.Jb, 74.72.−h

I. INTRODUCTION

The high-temperature superconducting cuprates (HTSs) are heterostructures at atomic limit made of stacks of CuO_2 atomic planes intercalated by spacer layers containing up to 25 percent of defects: oxygen interstitials, vacancies, or atomic substitutions. The simplest cuprate La_2CuO_4 (LCO) is made of a single layer CuO_2 intercalated by La_2O_2 rocksalt layers. The Fermi surface in La_2CuO_4 (LCO) is formed by a single band of the CuO_2 layer that crosses the Fermi level.[1] At half filling the Fermi surface is destroyed by electronic correlations making a charge transfer gap between Cu$3d^9$O$2p^6$ and Cu$3d^{10}$O$2p^5$ many-body electronic configurations. Insertion of dopants or defects in the spacer layers moves the chemical potential out of half filling, forming a complex metallic phase. The rigid band model predicts a Fermi surface (FS) made of a large cylinder.[1] The breakdown of the rigid band model in the underdoped phase is shown by the appearance of (i) Cu$3d^9$O$2p^5$ states in the charge transfer gap,[2] (ii) a pseudogap at the M point, (iii) the Fermi surface made of short arcs,[3] and (iv) an electron-like small FS pocket observed by quantum oscillations and the high-field Hall effect.[4] In the underdoped regime the homogeneous metallic phase competes with electronic phase separation with the formation of a complex heterogeneous phase.[5–8] The charge-spin ordering and electronic phase separation are accompanied by fluctuations of the local structure that diverges from the average structure.[9–14] The defects inserted in the spacer layers to dope the copper oxide electronic structure are an additional source for the modulation of the heterogeneous electronic states near the Fermi level.[15] Particular attention has been addressed to oxygen interstitials that are mobile because of the misfit strain between the active and spacer layers[16] inducing a contraction of the Cu-O bonds.[17] Controlling their ordering by thermal treatments giant effects on superconductivity have been reported.[18–20] Electronic structure calculations show that the displacement of apical oxygen, due to oxygen defects, changes the spin-phonon coupling[21] and the electronic states near the Fermi level in cuprates.[22] The control of the functional electronic properties via dopant manipulation is of very high interest in manganites[23] and graphene.[24] The focus has been recently addressed to the control of structural nanoscale phase separation into dopant-rich puddles embedded in a dopant-poor background in these complex materials. The dopant-rich puddles of ordered dopants have been clearly observed also in iron chalcogenide superconductors and it has been shown that the two structural units have a quite different electronic structure with a superconducting or a magnetic phase.[25–27] In the underdoped regime of cuprates a structural phase separation between a dopant-poor antiferromagnetic phase and a dopant-rich metallic phase with doping close to 1/8 is clearly observed in La_2CuO_{4+y} for $0< y <0.055$[28] and $YBa_2Cu_3O_{6+y}$.[29] In the optimum and high doping regime of cuprates recent high-resolution ARPES and STM experiments[30–32] show multiple electronic components with electronic phase separation at low temperature. A first pseudogap phase with doping around 1/8 competes with a highly doped metallic phase with about 1/4 holes per Cu

 ©2013 American Physical Society

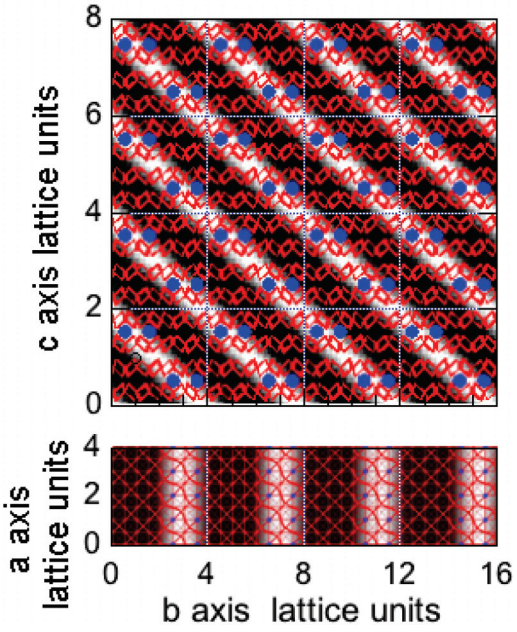

FIG. 1. (Color online) The ordering of oxygen interstitials (blue solid dots) in La214 in the (b,c) plane (upper panel) and in the (a,b) plane of the *Fmmm* structure as determined by x-ray diffraction using synchrotron radiation. The unit cell is $La_{16}Cu_8O_{32+N}$ with $N = 2$.

site well described band structure calculations, confirming previous findings of phase separation giving distinct physics beyond the superconducting dome.[10–12] Superoxygenated La_2CuO_{4+y}, $y > 0.08$, provides an ideal case to study the phase separation in the optimum doping regime and the role of ordering of oxygen interstitials (O_i's).[33–36] The O_i's in the rocksalt LaO layer are mobile; because of the large tensile strain in the spacer layers. This is due to the lattice misfit between different layers[16] of Cu-O bonds that is about 4% shorter than its equilibrium value of 1.97 Å.[17] Therefore, by thermal treatments it is possible to induce their three-dimensional ordering that has been shown to enhance the critical temperature to the highest value for La214.[35] The variation of the critical temperature of the heterogeneous sample depends both on self-organization of oxygen-rich puddles and on the ordering of oxygen interstitials, as has been shown using thermal treatments controlling T_c.[35] Using novel experimental microscopy, scanning nano x-ray diffraction, probing both the real and the k space, the formation of a granular phase in La_2CuO_{4+y} has been discovered. Metallic heavily doped puddles, with ordered oxygen interstitials in the spacer layers, are embedded in an oxygen-poor background[34–36] at optimal doping. In the heavily doped grains the excess oxygen interstitials are ordered as shown in Fig. 1 forming stripes along the [1,1,0] direction.

Despite such compelling pieces of evidence for the importance of oxygen order, there are no theoretical calculations on the electronic structure reconstruction near the Fermi level in the dopant-rich puddles. In this work we present electronic structure results for the highly hole doped puddles of ordered oxygen interstitial in superoxygenated La_2CuO_4. The method of calculation based on experimental structural information considers the supercells of O-rich LCO in Sec. II. In Sec. III we discuss the results of the calculations, and some ideas for future works are given together with the conclusions in Sec. IV.

II. METHOD OF CALCULATION

The calculations are made using the linear muffin-tin orbital (LMTO) method and the local spin-density approximation (LSDA). Electronic correlation can be disregard because the oxygen-rich puddles are very far from half filling. The details of the methods were published earlier.[37–42] The elementary cell of La_2CuO_4 (LCO) contains La sites at $(0,0,\pm 0.721c)$, Cu at (0,0,0), planar O's at (0.5,0,0) and (0,0.5,0), and apical O's at $(0,0,\pm 0.358c)$, in units of the lattice constant $a_0 = 3.8$ Å, where $c = 1.24$. In addition to the MT spheres at the atomic sites we insert MT spheres at positions $(0.5,0,\pm 0.5c)$ and $(0,0.5,\pm 0.5c)$ to account for the positions of empty spheres. The atomic sphere radii are 1.76 Å (La), 1.26 Å (Cu), 1.18 Å (planar O, O_i, and empty spheres), and 1.21 Å (apical O), respectively. The z projection of the corresponding irreducible Brillouin zone (BZ) is shown in Fig. 4(a) by the limiting points Γ-X-M, whereas the IBZ for the doubled cell ($La_4Cu_2O_8$) with ordered antiferromagnetic (AFM) order would be limited by Γ-X-M''. Eight units of the elementary cell La_2CuO_4 are put together to form a long supercell, $La_{16}Cu_8O_{32}$, with the generating lattice vectors $(1,-1,0),(4,4,0)$, and $(0.5,0.5,c)$, so that its axis is oriented parallel to the (1,1,0) direction, i.e., at 45° from the Cu-O bond direction along (1,0,0). The band calculations are made for this supercell containing 72 sites totally, where one or two of the empty sites at the interstitial positions are occupied by excess oxygen ions. These supercells are chosen in order to represent fairly well the experimentally determined structures.[34] A small lattice relaxation near oxygen interstitials is included in the first elementary segment of the supercell, so that apical O's are pushed away about $0.03a_0$ in the x-y plane. The basis set goes up through $\ell = 2$ for all sites. The z-projected IBZ corresponding to the supercell is shown in Fig. 4(a) by the limits Γ-M_3-X_3-R. Self-consistency is made with 192 k points and final results are based on 408 points in the IBZ.

No interstitial sites are occupied with O in one set of the calculations (called LCO-0). The DOSs of the LCO-0 calculations agree well with other published results on LCO.[1] The LCO-0 results serve as a reference for comparison with the results with oxygen interstitials. For instance, the FS for (lightly doped) LCO forms a circle centered at the M point in BZ of the elementary cell, but since the BZ corresponding to the supercell is folded and very flat along (1,1,0) it is necessary to identify the circle from several FS pieces in the folded zone. In two other sets of calculations we insert one ($La_{16}Cu_8O_{32+1}$, LCO-1) or two ($La_{16}Cu_8O_{32+2}$, LCO-2) oxygen ions at interstitial positions. In LCO-2 the two O are put at equivalent positions in two adjacent AFM cells, so that two stripes of O_i's, separated by $1.41a_0$, are formed along $\vec{x}$ (and $\vec{z}$).[34]

The excess O_i's sit at the interstitial interlayer positions, above the oxygen ion in the CuO_2 plane of the the orthorhombic unit cell, and form 3D ordered puddles below 350 K; see Fig. 1. The insertion of O_i's is expected to induce hole doping, because each new oxygen interstitial will bring 4 new bands well below E_F (one s and 3 p), but the oxygen has only 2 s and

4 p electrons. Therefore, simple arguments suggest that one Cu-O band becomes unfilled; i.e., E_F has to go down relative to the rest of the bands. However, this picture gets complicated by the fact that other atoms such as La serve as charge reservoirs, lattice reconstructions are likely, and in addition the excess O positions are ordered in stripelike patterns.[34]

It is often argued that correlation is too strong for having traditional bands in undoped cuprates when the Cu-d band is half filled.[43] On the other hand, ARPES (angular-resolved photoemission spectroscopy) and ACAR detect FS's and bands that evolve with doping and agree well with DFT (density functional theory) calculations.[1,3,44] Therefore, since we study doped cases here, it is not likely that correlation is more important than what is already included in our DFT calculations.

III. RESULTS AND DISCUSSION

The nonmagnetic (NM) total DOSs for $La_{16}Cu_8O_{32+N}$ near the Fermi level are shown in Figs. 2 and 3. It can be seen that the DOS is increasing considerably near E_F when one or two O_i's are added in form of stripes. The DOS difference between the cases $N = 0$ and $N = 2$ in Fig. 2(b) shows that most of the O_i-p bands fall in the interval $[-2.5,0]$ eV. Strong hybridization puts new states also on atoms around the O_i sites. The integrated differences [as the one shown in Fig. 2(c)] show that the electron count is about the same for all three cases at approximately -1.0 eV below the respective E_F's. The DOS at E_F, $N(E_F)$, increases roughly three times when two O's are added; see Table I. In the undoped sample the Fermi level E_F is well above the small peak in the DOS associated with the van Hove singularity. In the doped cases the peak in the total DOS splits forming two or three peaks separated by a partial gap slightly below E_F, so that E_F is tuned exactly at the top of one the DOS peaks. The DOS functions from individual bands near E_F show similar shapes, but within a narrower energy range when the number of O_i's increases. The partial band DOSs from bands 217–219 for $N = 2$ are displayed in Fig. 3(b). The shapes of the DOSs from bands 211–213 for

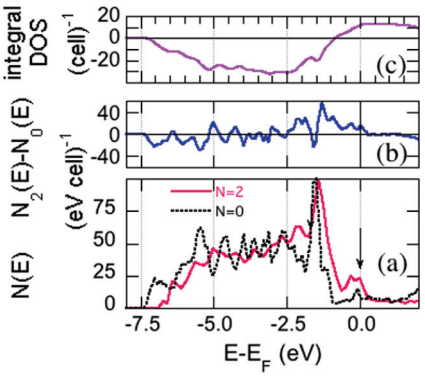

FIG. 2. (Color online) Lower panel: The total DOS for $La_{16}Cu_8O_{32+N}$ with $N = 0$ and $N = 2$. A broadening with a FWHM of ~0.01 eV is included. Middle panel: The difference of the DOS for $N = 2$ minus the DOS for $N = 0$. The maximum at -2 eV indicates the main energy location of the O($2p$) impurity states of oxygen interstitial. Upper panel: The number of states, i.e., the integrated value of what is shown in the middle panel.

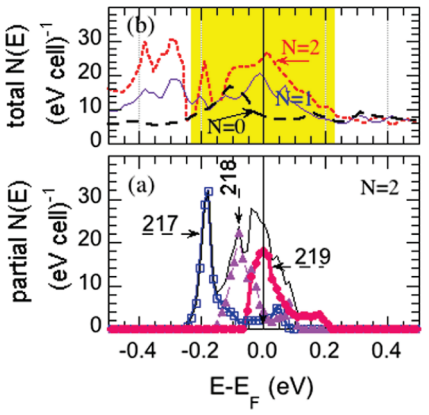

FIG. 3. (Color online) Upper panel: The total DOS for different bands near E_F in $La_{16}Cu_8O_{32+N}$ for $N = 0$, 1, and 2, with a broadening of about 5 meV. Lower panel: The partial DOS of the 3 minibands crossing E_F in $La_{16}Cu_8O_{32+2}$ and their sum (thin line) with broadening of about 3 meV. The Fermi energy of the upper miniband (219) is only 60 meV, to be compared with a superconducting gap of the order of 30 meV. The Fermi energy of the other two minibands (218, 217) are 150 meV and 240 meV. The Fermi energy of the corresponding bands (213–211 in the undoped case) for $N = 0$ is about 180, 300, and 950 meV, respectively. The gap between the 219 and 218 minibands, about 80 meV, is of the same order of magnitude as the so-called pseudogap in the antinodal point of the Fermi surface.

$N = 0$ look similar, but are ~3 times wider. Only three bands have a significant $N(E_F)$; see also Table I. The two bands that contribute most to the total E_F are the middle and upper bands, 218 and 219, for $N = 2$ (and 212 and 213 for $N = 0$, and 215 and 216 for $N = 1$). These upper bands hybridize with O_i and make the local DOS on the added O very high, about twice as high as the local d DOS on Cu. The local Cu-d DOS is largest on Cu sites near the O_i's (typically twice the DOS on Cu far from O_i). On the average there is a quite delocalized increase of the Cu-d DOS coming from the uppermost band when oxygen interstitials are added. This increase is smaller than of the total DOS, because of the large O-p DOS, but it is most striking for the upper band, suggesting that this band is most important for any benefit of superconducting properties.

The changes of the effective charges (see Table I) show a weak hole doping on Cu when the number of O_i increases. A weak doping is also seen on the planar O charges in agreement with experiments showing only about one hole per Cu site induced by each oxygen interstitial at high doping. The charge

TABLE I. Total and band decomposition of the DOS at E_F in units of (cell eV)$^{-1}$, and average charges within each MT sphere of the different atoms, in units of valence electrons per atom. Only 3 bands have a significant DOS at E_F; see the text for the numbering of the 3 bands in each case. The charges on Cu and especially La differ from site to site depending on the proximity to interstitial O. The O charges are averaged planar and apical O and do not include the O_i's.

	$N(E_F)$	Low	Mid	Upper	Q_{Cu}	Q_{La}	Q_O
LCO-0	8	1.5	3.0	4.2	10.23	7.86	6.43
LCO-1	20	3.5	4.8	12	10.19 ± 0.02	7.92 ± 0.14	6.43
LCO-2	25	3.0	3.7	18	10.15 ± 0.02	7.98 ± 0.13	6.42

on O_i is ∼0.15 electrons less than within an apical O of the same volume. This difference makes the 1*s* core levels to go up by about 1.5 eV on O_i compared to the other O.

The FS of undoped LCO consists of a rather 2-dimensional almost circular cylinder with origin at the *M* point. The radius of the cylinder is quite large so that the FS englobes the M'' point in the center; see the schematic FS in Fig. 4(a). The radius gets larger for increasing doping and the FS reaches the *X* and *Y* points at optimal doping when E_F coincides with the van Hove singularity peak in the DOS. AFM order on Cu sites leads to a cell doubling and the BZ is folded along the *X*-*Y* line to obtain the irreducible part of the AFM-BZ within Γ-*X*-M''. One portion of the FS will be folded into the section "b" in Fig. 4(a), while "a" is already within the AFM-BZ. Our band calculations are made for a 4 times extension of the AFM cell in the (1,1,0) direction, and the corresponding BZ is found from two more foldings of the AFM BZ, the first at the line M_2-X_2 and once more at M_3-X_3. The new irreducible BZ is confined within Γ-M_3-X_3-*R*, and the portions "d," "c," and "e" constitute the down-folded FS circle of the elementary BZ into the BZ for the supercell. These 3 bands are found at E_F in the supercell calculations for LCO-0 and LCO-2 as can be seen in Figs. 4(b) and 4(c). Fluctuations tend to open a gap at the point "1."[42,45,46] It is also realized that portions "e" and parts of "c" will be gone at high doping. This is because the original *M*-centered FS circle will increase its radius for higher doping; the FS crossing that occurs on the *M*-*X* line for low doping will reach the *X* point at optimal doping, and ultimately cross the Γ-*X* line when the doping is increased further. The traces of the "e" and "c" portions will also be gone if there is a gap of the original FS at *X*, i.e., if the FS circle in the elementary BZ breaks up into a banana-shaped feature centered at M''.

In Figs. 4(b) and 4(c) are displayed the FS pieces in the $k_z = 0$ planes of the irreducible BZ for $N = 0$ and 2. For the calculations without interstitial O it is easy to recognize the FS model in the real FS in the $k_z = 0$ plane. There are minor modifications in other k_z planes because of a weak 3D dispersion. The energy window is set narrower for the results with 2 interstitial O's in order to avoid too many points for the more flat bands in this case. Many of the same structures of the FS are seen in the plots for the results with interstitial O's as for the results without them. But two differences draw our attention: First, there are many FS points (this is more striking when the same energy window is used as for the undoped cell) to the left of the panel, close to Γ, when there are O interstitials, which suggests that mainly the FS piece "d" in Fig. 4 has gained a higher DOS. This agrees with the high DOS for the upper band (219 for $N = 2$). In addition, section "d" is closer to the M_3-X_3 line, indicating hole doping as for an enlarged unfolded FS circle. Second, no FS is seen to the right (i.e., at $k_p = 0.5$) for $N = 2$, which probably means that a gap has opened near the *X* point, or that the effective doping is such that the original unfolded FS already is beyond the *X* point. A separate small hole pocket appears near $k_x \sim 0.45$. An effort to force a back folding of that pocket into the original zone would put that band close to *X* on the M''-*X* line. The possibility of a gap at *X* is interesting, since a pseudogap is often associated with enhanced T_c near optimal doping for conventionally doped LSCO, and a small pocket nearby sets up the condition for the Lifshitz mechanism.[47] Such band features can to some extent

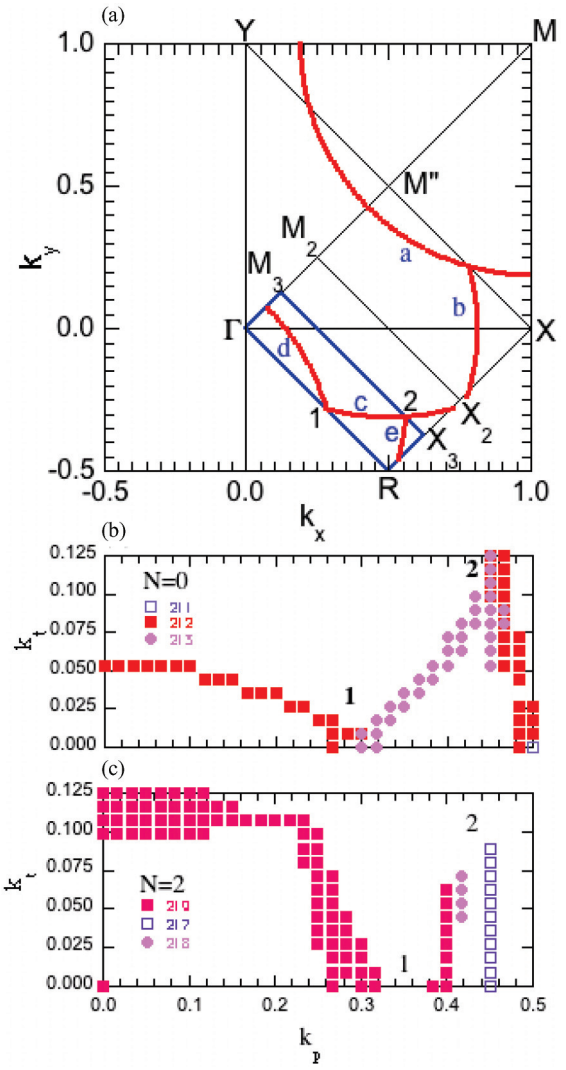

FIG. 4. (Color online) (a) A schematic view of how a circular *M*-centered FS in the normal BZ (the irreducible part is limited by Γ-*X*-*M*) is folded into the BZ of the supercell given by the rectangle Γ-M_3-X_3-*R*. The M'' is halfway between Γ and *M* and Γ-*X*-M'' is the limit of the basic AFM BZ. (b) The FS pieces (bands 211–213) in the $k_z = 0$ planes of the irreducible BZ (i.e., within Γ-M_3-X_3-*R*) for $N = 0$. (c) The FS pieces (bands 217–219) in the $k_z = 0$ planes of the irreducible BZ for $N = 2$.

be understood; a dispersive band in the [1,1,0] direction breaks up by the new periodicity and the band becomes flat at the limit of the (shortened) BZ where even small gaps might appear. The DOS will be large if the band remains flat in other *k* directions. It is a matter of tuning the periodicity to the doping so that E_F coincides with a favorable structure in the DOS.[41] It has been demonstrated that the pseudogap depends on stripelike potential modulations in the (1,0,0) direction, as from phonon or spin waves,[37,39,40] but here the stripes are oriented in the (1,1,0) direction. These features are a bit different when only one oxygen interstitial is added.

A high DOS is normally connected with strong spin fluctuations. It has been shown that for a certain correlation between the wavelength of spin fluctuations and the doping, the pseudogap can open right at E_F, where also phonons can

TABLE II. Local Stoner enhancement S and within parentheses the induced local moment (m in units of μ_B/atom) on 4 Cu calculated for AFM fields of ±5 mRy. The two first Cu are closest to the interstitial O, while Cu(3) and Cu(4) far from them are most disposed to show magnetism. Distortion in one layer of apical O and unequal distances to interstitial O in LCO-2 contribute to differences between Cu sites.

	Cu(1) S (m)	Cu(2) S (m)	Cu(3) S (m)	Cu(4) S (m)
LCO-0	1.46 (0.061)	1.46 (−0.060)	1.46 (−0.060)	1.46 (0.060)
LCO-1	1.51 (0.063)	1.42 (−0.050)	1.62 (−0.079)	1.63 (0.081)
LCO-2	1.45 (0.060)	1.45 (−0.059)	1.43 (−0.055)	1.56 (0.071)

contribute.[21,39] Now the modulation is in the (1,1,0) direction without optimization of the length of the supercell to the doping, but it is still of interest to see whether AFM spin fluctuations can become stronger by interstitial O's. This is seen from spin-polarized calculations where AFM fields are applied to Cu atoms to create a spin wave along the cell. Two pairs of Cu's near and far from the O_i's have the applied fields (±5 mRy), while other Cu's at the nodes of the wave have no applied field. The local exchange enhancement (Stoner factor) and moments will be the measure of the strength toward spin fluctuations.

The results are summarized in Table II. As seen, with extra O_i's the tendency is such that the local enhancements are larger on sites far from the oxygen interstitial, on sites where the DOS is not highest. The DOS on Cu near oxygen interstitial is increased by direct hybridization with p states on those O sites. The local O-p DOS near E_F is large on O_i (larger than 1 eV^{-1}) and nearby apical O (0.5–1 eV^{-1}), which is in contrast to the case without interstitial O or far away from the O_i where the DOS is small (less than 0.1 eV^{-1}). This fact works against an enhancement on Cu, because the Cu-d and O-p bands are tightly bound and the latter are less adapted for magnetism.

IV. CONCLUSION

Oxygen interstitials added in the form of stripes in the spacer layers form three overlapping minibands crossing E_F making the DOS larger and E_F appears at the maximum of one of the DOS peaks. Thus, the natural growth of O_i stripes in the oxygen-rich puddles seems to be an efficient way to generate potential modulations for having E_F on a DOS peak with high $N(E_F)$, accompanied by enlarged electron-phonon coupling and T_c.[41] There are many possibilities for spectroscopic verification of the local electronic structure near the interstitials. It would be very important to perform ARPES measurements using photon excitation beams focused on nanoscale spots to measure the electronic structure of the super-oxygenated puddles calculated here. It is clear that ARPES experiments using large photon beams give information on the spatially averaged structure probing at the same time both oxygen-rich and oxygen-poor domains. Therefore we propose that nanofocused photoemission experiments would be a powerful probe to detect band narrowing in oxygen ordered O_i's. The fact that we find an upward shift of the O-1s core level of the order 1.5 eV on the single stripe of O_i and nearby apical O (compared to the O far from the interstitials) suggests that the increase of local O_i-p DOS can be detected via the threshold energies of soft x-ray emission and/or absorption spectroscopy. The more than tenfold increase of the local p DOS near E_F on interstitials is a large effect that should modify spectroscopic intensities as a function of increased oxygen content.

The changes of electronic structure on Cu sites are strong and moderately favorable to AFM spin fluctuations with possibilities for enhanced λ_{spin}. Furthermore, there is a segmentation of the original FS with a superconducting puddles, into smaller disconnected pockets, from which the shape resonance in the superconducting gaps near a Lifshitz transition emerges as an additional mechanism for high T_c.[47,48] We show that the ordered lattice with 3D oxygen interstitials in oxygen-rich puddles in LCO provides a realization of multiband metallic puddles. All calculated features of the electronic structure of the oxygen-rich nanopuddle are expected to be favorable to enhance superconductivity; however, the comparison with experimental methods probing the average electronic structure of cuprates will require the study of networks of superconducting multiband puddles described in this paper. Finally theoretical works on HTSs focusing on granular superconductors,[49,50] where the maximum superconducting critical temperature occurs at a critical density for the superconductor-insulator transition in a network of 2d percolation clusters,[51] could investigate networks of multiband superconducting puddles for understanding many puzzles of high-temperature superconductors.

[1] W. E. Pickett, Rev. Mod. Phys. **61**, 433 (1989).
[2] A. Bianconi, A. Congiu-Castellano, M. De Santis, P. Rudolf, P. Lagarde, A. M. Flank, and A. Marcelli, Solid State Commun. **63**, 1009 (1987).
[3] A. Damascelli, Z.-X. Shen, and Z. Hussain, Rev. Mod. Phys. **75**, 473 (2003).
[4] D. LeBoeuf, N. Doiron-Leyraud, B. Vignolle, M. Sutherland, B. J. Ramshaw, J. Levallois, R. Daou, F. Laliberte, O. Cyr-Choiniere, J. Chang, Y. J. Jo, L. Balicas, R. Liang, D. A. Bonn, W. N. Hardy, C. Proust, L. Taillefer *et al.*, Phys. Rev. B **83**, 054506 (2011).
[5] J. Zaanen, Nature (London) **466**, 825 (2010).
[6] L. P. Gor'kov and G. B. Teitel'baum, J. Phys.: Conf. Ser. **108**, 012009 (2008); Phys. Rev. Lett. **97**, 247003 (2006).
[7] K. I. Kugel, A. L. Rakhmanov, A. O. Sboychakov, N. Poccia, and A. Bianconi, Phys. Rev. B **78**, 165124 (2008).
[8] V. Kresin, Y. Ovchinnikov, and S. Wolf, Phys. Rep. **431**, 231 (2006).
[9] A. Bianconi, Solid State Commun. **89**, 933 (1994).
[10] A. Bianconi, Physica C **235–240**, 269 (1994).
[11] A. Bianconi and M. Missori, Solid State Commun. **91**, 287 (1994).
[12] A. Bianconi, M. Missori, H. Oyanagi, H. Yamaguchi, D. H. Ha, Y. Nishiara, and S. Della Longa, Europhys. Lett. **31**, 411 (1995).

[13]A. Bianconi, N. L. Saini, A. Lanzara, M. Missori, T. Rossetti, H. Oyanagi, H. Yamaguchi, K. Oka, and T. Ito, Phys. Rev. Lett. **76**, 3412 (1996).
[14]T. Egami and S. J. L. Billinge, *Underneath the Bragg Peaks* (Pergamon, Oxford, 2003).
[15]P. Littlewood, Nat. Mater. **10**, 726 (2011).
[16]A. Bianconi, S. Agrestini, G. Bianconi, D. Di Castro, and N. L. Saini, J. Alloys Compd. **317-318**, 537 (2001).
[17]J. Garcia, A. Bianconi, M. Benfatto, and C. R. Natoli, Colloq. Phys. **47**, C8 (1986).
[18]P. W. Barnes, M. Avdeev, J. D. Jorgensen, D. G. Hinks, H. Claus, and S. Short, Phys. Rev. B **72**, 134515 (2005).
[19]T. H. Geballe and M. Marezio, Physica C **469**, 680 (2009).
[20]O. Chmaissem, I. Grigoraviciute, H. Yamauchi, M. Karppinen, and M. Marezio, Phys. Rev. B **82**, 104507 (2010).
[21]T. Jarlborg, Phys. Rev. B **68**, 172501 (2003).
[22]T. Jarlborg, B. Barbiellini, R. S. Markiewicz, and A. Bansil, Phys. Rev. B **86**, 235111 (2012).
[23]B. Bryant, C. Renner, C. Tokunaga, Y. Tokura, and G. Aeppli, Nat. Commun. **2**, 212 (2011).
[24]T. O. Wehling, M. I. Katsnelson, and A. I. Lichtenstein, Phys. Rev. B **80**, 085428 (2009); T. O. Wehling, K. S. Novoselov, S. V. Morozov, E. E. Vdovin, M. I. Katsnelson, A. K. Geim, and A. I. Lichtenstein, Nano Lett. **8**, 173 (2007).
[25]W. Li, H. Ding, P. Deng, K. Chang, C. Song, K. He, L. Wang, X. Ma, J.-P Hu, X. Chen, and Q.-K Xue, Nat. Phys. **8**, 126 (2011).
[26]A. Ricci, N. Poccia, G. Campi, B. Joseph, G. Arrighetti, L. Barba, M. Reynolds, M. Burghammer, H. Takeya, Y. Mizuguchi, Y. Takano, M. Colapietro, N. L. Saini, and A. Bianconi, Phys. Rev. B **84**, 060511 (2011); A. Ricci, N. Poccia, B. Joseph, G. Arrighetti, L. Barba, J. Plaisier, G. Campi, Y. Mizuguchi, H. Takeya, Y. Takano *et al.*, Supercond. Sci. Technol. **24**, 082002 (2011).
[27]V. Ksenofontov, G. Wortmann, S. A. Medvedev, V. Tsurkan, J. Deisenhofer, A. Loidl, and C. Felser, Phys. Rev. B **84**, 180508 (2011).
[28]P. G. Radaelli, J. D. Jorgensen, R. Kleb, B. A. Hunter, F. C. Chou, and D. C. Johnston, Phys. Rev. B **49**, 6239 (1994).
[29]G. Campi, A. Ricci, N. Poccia, L. Barba, G. Arrighetti, M. Burghammer, A. S. Caporale, and A. Bianconi, Phys. Rev. B **87**, 014517 (2013).
[30]I. M. Vishik, M. Hashimoto, R.-H. He, W.-S. Lee, F. Schmitt, D. Lu, R. G. Moore, C. Zhang, W. Meevasana, T. Sasagawa *et al.*, Proc. Natl. Acad. Sci. USA **109**, 18332 (2012).
[31]W. S. Lee, I. M. Vishik, K. Tanaka, D. H. Lu, T. Sasagawa, N. Nagaosa, T. P. Devereaux, Z. Hussain, and Z. X. Shen, Nature (London) **450**, 81 (2007).
[32]A. Piriou, N. Jenkins, C. Berthod, I. Maggio-Aprile, and O. Fischer, Nat. Commun. **2**, 221 (2011).
[33]H. E. Mohottala, B. O. Wells, J. I. Budnick, W. A. Hines, C. Niedermayer, L. Udby, C. Bernhard, A. R. Moodenbaugh, and F.-C. Chou, Nat. Mater. **5**, 377 (2006).
[34]M. Fratini, N. Poccia, A. Ricci, G. Campi, M. Burghammer, G. Aeppli, and A. Bianconi, Nature (London) **466**, 841 (2010).
[35]N. Poccia, M. Fratini, A. Ricci, G. Campi, L. Barba, A. Vittorini-Orgeas, G. Bianconi, G. Aeppli, and A. Bianconi, Nat. Mater. **10**, 733 (2011).
[36]N. Poccia, A. Ricci, G. Campi, M. Fratini, A. Puri, D. Di Gioacchino, A. Marcelli, M. Reynolds, M. Burghammer, N. Saini, G. Aeppli, and A. Bianconi, Proc. Natl. Acad. Sci. USA **109**, 15685 (2012).
[37]T. Jarlborg, Phys. Rev. B **64**, 060507(R) (2001).
[38]B. Barbiellini and T. Jarlborg, Phys. Rev. Lett. **101**, 157002 (2008).
[39]T. Jarlborg, Phys. Rev. B **76**, 140504(R) (2007).
[40]T. Jarlborg, Physica C **454**, 5 (2007).
[41]T. Jarlborg, Appl. Phys. Lett. **94**, 212503 (2009).
[42]T. Jarlborg, Phys. Rev. B **84**, 064506 (2011).
[43]P. Fulde, *Electron Correlations in Molecules and Solids* (Springer-Verlag, Berlin, 1993).
[44]B. Barbiellini, P. Genoud, J. Y. Henry, L. Hoffmann, T. Jarlborg, A. A. Manuel, S. Massidda, M. Peter, W. Sadowski, H. J. Scheel, A. Shukla, A. K. Singh, and E. Walker, Phys. Rev. B **43**, 7810 (1991).
[45]N. Harrison, R. D. McDonald, and J. Singleton, Phys. Rev. Lett. **99**, 206406 (2007).
[46]J. Meng, G. Liu, W. Zhang, L. Zhao, H. Liu, X. Jia, D. Mu, S. Liu, X. Dong, J. Zhang, W. Lu, G. Wang, Y. Zhou, Y. Zhu, X. Wang, Z. Xu, C. Chen, and X. Zhou, Nature (London) **462**, 335 (2009).
[47]D. Innocenti, S. Caprara, N. Poccia, A. Ricci, A. Valletta, and A. Bianconi, Supercond. Sci. Technol. **24**, 015012 (2011); A. Perali, A. Bianconi, A. Lanzara, and N. L. Saini, Solid State Commun. **100**, 181 (1996).
[48]D. Innocenti, N. Poccia, A. Ricci, A. Valletta, S. Caprara, A. Perali, and A. Bianconi, Phys. Rev. B **82**, 184528 (2010).
[49]E. V. L. de Mello, Europhys. Lett. **98**, 57008 (2012).
[50]G. Bianconi, Phys. Rev. E **85**, 061113 (2012); J. Stat. Mech.: Theory Exp. (2012) P07021.
[51]G. Bianconi, Europhys. Lett. **101**, 26003 (2013).